Journal Pre-proofs

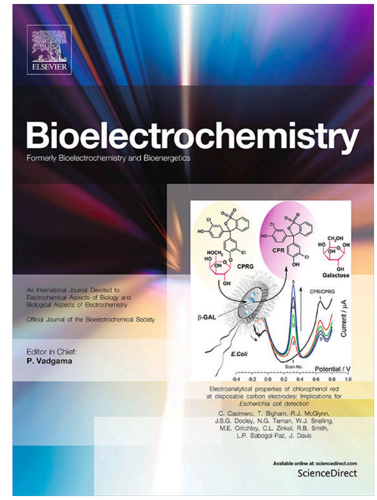


# The Effect of Anode Hydrodynamics on the Sensitivity of Microbial Fuel Cell Based Biosensors and the Biological Mechanism

Yue Yi, Beizhen Xie, Ting Zhao, Ziniu Qian, Hong Liu

PII: S1567-5394(19)30405-0
DOI: https://doi.org/10.1016/j.bioelechem.2019.107351
Reference: BIOJEC 107351

To appear in: *Bioelectrochemistry*

Received Date: 24 June 2019
Revised Date: 26 August 2019
Accepted Date: 26 August 2019

Please cite this article as: Y. Yi, B. Xie, T. Zhao, Z. Qian, H. Liu, The Effect of Anode Hydrodynamics on the Sensitivity of Microbial Fuel Cell Based Biosensors and the Biological Mechanism, *Bioelectrochemistry* (2019), doi: https://doi.org/10.1016/j.bioelechem.2019.107351

# The Effect of Anode Hydrodynamics on the Sensitivity of Microbial Fuel Cell Based Biosensors and the Biological Mechanism

Yue Yi[a,b,c], Beizhen Xie[a,b,c], Ting Zhao[a,b,c], Ziniu Qian[a,b,c], Hong Liu[a,b,c,*]

[a] Beijing Advanced Innovation Center for Biomedical Engineering, Beihang University, Beijing 100083, China

[b] Institute of Environmental Biology and Life Support Technology, School of Biological Science and Medical Engineering, Beihang University, Beijing 100083, China

[c] International Joint Research Center of Aerospace Biotechnology & Medical Engineering, Beihang University, Beijing 100191, China



[*] Corresponding author: Hong Liu, PhD, Professor, School of Biological Science and Medical Engineering, Beihang University, 37 Xueyuan RD, Haidian DIST, Beijing 100083, China.
Tel./fax: +86-10-82339837; e-mail: LH64@buaa.edu.cn

Abstract: Fluid dynamics in the anodic chamber of a microbial fuel cell (MFC) is a key factor affecting the distribution of substrates and the efficiency of mass transport. However, the effect of hydrodynamics on MFC based biosensor (MFC-Biosensor) sensitivity has not been established. In this study, the three-dimension anode flow field of a two chamber MFC was visualized, and anodic configuration optimized by a reasonable serpentine flow field and inlet/outlet settings. Through optimization, the proportion of the dead zone in the anodic configuration decreased by 14.1%, and the velocity at the anode surface increased by 334.6% with better homogeneity of distribution. Moreover, electricity production and sensitivity for the detection biotoxicity at MFC-Biosensors improved by 23.1% and 46.1-52.3%, respectively. Biofilm viability analysis further proved that the enhanced surface velocity was of benefit for the permeation of toxicants into anodic biofilms, thus improving the sensor performance.

Keywords: microbial fuel cell; biosensor; fluid field; hydrodynamic characteristic; biofilm viability.

## 1. Introduction

A Microbial fuel cell (MFC) is a device which can convert chemical energy in organic matter into electricity by catalysis of electricigens [1]. This novel bioelectrochemical technology, makes it feasible to achieve improvement of wastewater treatment efficiency and recovery of energy simultaneously, and is considered a promising solution to address the problems of excessive energy consumption and the wastage of resource during sewage treatment [2, 3]. However, relatively high manufacturing costs and poor electricity generation performance are the main bottlenecks restricting the application of MFC technology in real world wastewater treatment. Alternatively, MFCs can be employed to serve as biosensors for water quality monitoring, regardless of the power production insufficiency. Previous studies have confirmed the feasibility of using MFCs to assess biological oxygen demand [4, 5], nitrate [6], pathogen [7], biotoxicity [8-11] in water. Amongst these water quality parameters, the on site and on line biotoxicity monitoring by an MFC based biosensor (MFC-Biosensor) has attracted broad attention, and extensive research has been conducted to improve sensor performance [12, 13]. Compared with other conventional biosensors, MFC-Biosensors can achieve faster detection of water quality without additional signal transduction devices, and thus are expected to be one of the more promising applications of MFCs [14].

Relatively poor sensitivity is a major challenge for the development of MFC-Biosensors [14]. For on line monitoring, the continuous flow of pretreated water through an anodic chamber is indispensable during the detection process of an MFC-Biosensor. Therefore, the flow pattern of an anodic fluid may be one of the key parameters affecting sensor sensitivity. Previous studies have reported the effects of hydrodynamic characteristics on the electrical performance of MFCs and the pollutant removal efficiency [15, 16]. Through conventional residence time distribution tests (*i.e.* tracer tests), the liquid flow characteristics of membrane-less MFCs with two different anode structures were revealed [17]. It was found that a perforated graphite felt sheet instead of a normal graphite felt sheet largely reduced the occurrence of short-circuiting and thus enhanced the MFC output current. Furthermore, computational fluid dynamics (CFD) simulation was employed to visualize the flow pattern inside an electrochemical membrane bioreactor (EMBR) and to investigate the effect of hydraulic retention time (HRT) on the dead volume of the EMBR [18]. The results acquired by CFD simulation were in accordance with those of tracer tests, and an optimized HRT setting reduced the volume of dead zone and further promoted electricity generation [18]. These studies suggest that appropriate hydrodynamic properties are crucial to improve MFC electricity generation performance and the underlying mechanisms may be the better distribution of substrates [19] and the enhancement of mass transport [20]. Therefore, the hydrodynamic characteristics in an anodic chamber might also affect the water quality monitoring by an anodic biofilm, thus affecting the sensitivity of an MFC-Biosensor.

Only a little published research has reported the effects of hydrodynamic characteristics on MFC-Biosensor performance. Massaglia *et al.* compared the sensor performance of a squared shape and a drop-like shape MFC-Biosensors for the quantification of organic matter [21]. They found that the drop-like shape one delivered more rapid response and higher sensitivity due to the larger percentage of effective exposed area shown by CFD simulation [21]. This result suggests that the effective flow in an anodic chamber is a possible factor affecting sensor sensitivity. Additionally, another study investigated the influence of anodic configuration on Cu[II] detection using MFC-Biosensors. It was observed that the sensitivity for Cu[II] monitoring increased by ~15–41 times with the adoption of a flow-through electrode instead of a flow-by one, and the enhanced sensitivity might be attributed to the promoted mass transport of Cu[II] ions [22], which indicates the important role of anode surface velocity to sensor performance. Moreover, recent studies have revealed that the velocity distribution at the anode surface also impact the sensitivity of an MFC-based sodium acetate sensor [15, 23]. On the other hand, hydrodynamic characteristics largely depend on the configuration of an anodic chamber [24]. Early studies have proved that a serpentine flow field can significantly enhance the sewage treatment efficiency of a bioreactor [15, 25], and different inlet/outlet settings also have obvious effects on MFC electricity performance [20]. Nevertheless, each previous study only considered the effect of a single characteristic on MFC performance. Complex impacts of these hydrodynamic parameters on MFC performance and sensor sensitivity have not be investigated and revealed.

In the majority of published literatures, the visualization of the flow patterns inside MFC anodic chambers was acquired by two-dimension (2-D) CFD simulation and the permeability of anode was neglected, which resulted in a rough estimation of the velocities at the anode surfaces. To address these limitations, three-dimension (3-D) CFD simulation was employed in this study, and dead zone percentages as well as surface velocities were quantified more accurately. Then, orthogonal tests were conducted to investigate the effects of a serpentine flow field and inlet/outlet positions on anode hydrodynamics. Additionally, MFC-Biosensors with an original configuration and an optimal configuration were constructed respectively to compare the sensor sensitivity for acute toxic shocks. The underlying biological mechanism was finally investigated by the combination of biofilm viability analysis and CFD results.

## 2. Materials and Methods

### 2.1 Basic equations

Reynolds number (Re) is defined as the ratio between inertial force and viscous force into a fluid [26]. Here Re was used to differentiate between a laminar flow and a turbulent flow, and Re can be calculated according to Eq. (1):

$$\mathrm{Re} = \rho v d/\mu \quad (1)$$

where ρ is the fluid density ($kg \cdot m^{-3}$), v is the fluid velocity ($m \cdot s^{-1}$), d is the characteristic fluidic length (m), and μ is the viscosity of a fluid ($kg \cdot m^{-1} \cdot s^{-1}$). For a fluid with a non-circular cross-section, d equals to hydraulic diameter and is defined as Eq. (2):

$$d = 4A/p \quad (2)$$

where A is the cross-sectional area ($m^2$), and p is the wetted perimeter (m). Similar to the previous literatures [20, 21], the density and viscosity of anolyte was assumed to be those of liquid water. Considering that the inlet flow rate of anolyte was only 3 mL/min in this study, the estimated value of Re was less than 100. Thus, the anodic fluid was considered as a laminar flow.

The fluid field inside the anodic chamber was divided into two regions. One was the region where the anode (carbon cloth in this study) located and was denoted as the porous domain due to the porous structure of the carbon cloth. The other region covered the rest part of the anodic interior and was denoted as the non-porous domain. For the nonporous domain, the Navier-Stokes equation, which describes the momentum conservation of a viscous fluid, was used to model the motion of anolyte and is defined as follows:

$$\rho(v \cdot \nabla v) = -\nabla P + \rho g + \mu \nabla^2 v \quad (3)$$

where v is the velocity ($m \cdot s^{-1}$), P is the pressure (N), and g is the gravitational acceleration ($m \cdot s^{-2}$).

For the porous domain, the effect of a porous medium on a viscous Newtonian fluid flow depends on the porosity and permeability of the medium, which can be described by the Navier-Stokes-Brinkman formulation [27]:

$$\rho \frac{v \cdot \nabla v}{\varepsilon^2} = -\nabla P + \rho g + \frac{\mu \nabla^2 v}{\varepsilon} - \frac{\mu v}{k} \quad (4)$$

where ε and 1/k are the porosity and the viscous resistance coefficient ($m^{-2}$) of a porous medium, respectively.

The continuity of a steady and incompressible flow in an anodic chamber can be described as Eq. (5):

$$\nabla \cdot v = 0 \quad (5)$$

### 2.2 3-D CFD simulation of anodic fluid field

A dual-chamber MFC with an additional reference electrode was designed based on our previous study [28], and it was denoted as the original MFC. Both the anodic and cathodic chambers had a cubic structure and a cylindrical interior. The radii of the interiors were both 15 mm, and the depths were 25 mm and 50 mm for the interiors of anodic and cathodic chambers, respectively. The working volume of the anodic chamber was 20 mL while it was 40 mL for the cathodic chamber. A proton exchange membrane (Nafion 117, DuPont Co., Ltd, USA) was used to prevent short-circuit. A 20 mm × 20 mm × 0.32 mm piece of carbon cloth (HCP330, Hesen Electric Co., Ltd, China) was placed in the center of the anodic chamber as anode. Two 20 mm × 20 mm × 0.1 mm pieces of 0.5 mg·cm$^{-2}$ Pt-loaded carbon paper (HCP120, Hesen Electric Co., Ltd, China) were inserted in the cathodic chamber to support cathodic oxygen reduction reaction. An additional Ag/AgCl reference electrode was used to operate the MFC under a constant anode potential mode during biosensor tests [29]. The inlet and outlet of the anodic chamber were located at the center of its bottom and top with the same inner diameter of 6 mm.

Considering that the anode flow field of the original MFC was symmetrical, a symmetry plane was set and only a half of the flow field was constructed for CFD simulation. The CFD simulation was performed with following steps. Firstly, the 3-D geometric model of the half flow field was constructed using AutoCAD 2016 (Autodesk Inc., USA) and was imported into Design Modeler (Ansys Inc., USA) to define its inlet, outlet and symmetry plane. Then, the computational grids of the model were generated using Mesh module (Ansys Inc., USA), and the independency of the grids was checked. After that, the grids were imported into Fluent (Ansys Inc., USA) to simulate the anodic fluid flow. As mentioned above, the nonporous domain was regarded as liquid water while the porous domain was simulated with a porous media model. The porosity of the model was set as 0.755 based on the mercury intrusion test result of the carbon cloth (data not shown) [30]. The viscous resistance coefficient was calculated according to a previous report [31] and was set as 1.1437E+11 m$^{-2}$. The inertial resistance coefficient of the porous medium was set as 0 m$^{-1}$ [18]. Moreover, a pressure-based solver and a laminar flow model were used, respectively, due to the incompressible and laminar properties of the anodic fluid flow [32]. As for boundary conditions, the inlet was applied to a mass-flow-inlet condition while the outlet was applied to a free outflow condition. The detailed parameters used in the CFD simulation are shown in supplementary materials, and the simulation results and flow visualization were obtained using CFD-post (Ansys Inc., USA).

2.3 Optimization of MFC configuration

Inlet/outlet locations, serpentine flow fields and their interaction are considered to be the main factors affecting the anodic fluid field. Therefore, a four-factor, three-level orthogonal experiment was designed to determine the optimal combination of inlet/outlet locations and baffle settings. The four factors, including the distance from the inlet to one edge ($L_a$, equals to the distance from the outlet to the other edge), the baffle lengths ($L_e$), the baffle gradient ($G_r$) and the distance from the baffle to the anode ($L_b$), are shown in Schematic 1, and each factor has three levels. Considering the possible interaction between $L_a$ and $L_e$, a total of eighteen geometric models were tested according to orthogonal design. Then, the hydrodynamic characteristics of each model, including the percentage of the dead zone inside the anodic flow field ($d_p$), the average value ($w_{min}$) and the variable coefficient ($v_c$) of the velocity at the anode surface, were obtained and were weighted to provide a comparison among the models. Finally, range analysis was used to determine the optimal configuration.

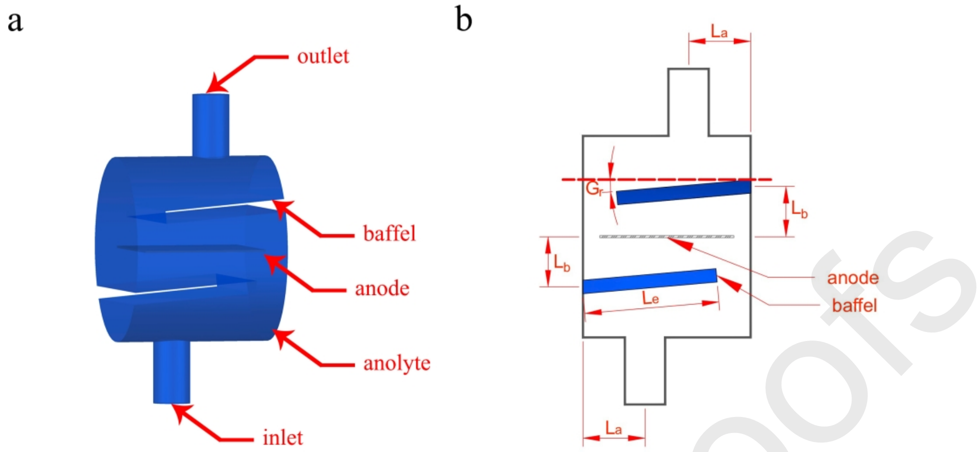


Schematic 1 Schematic of the optimization strategy (a) and the optimized factors (b).

## 2.4 MFC construction and start up

According to the results of the orthogonal test, two MFCs with the optimal configuration (denoted as the optimal MFCs) as well as two original MFCs were constructed to investigate the effect of anodic configuration on MFC performance. After fabrication, all the MFCs except for the Ag/AgCl electrodes were autoclaved. The Ag/AgCl electrodes were soaked overnight in 75% alcohol and sterilized with ultraviolet radiation [33]. Then all the MFCs were inoculated with *Shewanella loihica* PV-4 (ATCC®BAA-1088™, ATCC, USA) at the same inoculation ratio (30% v/v) and then filled with sterile anolyte in a laminar flow cabinet (SW-CJ-1F, Airtech, China). The anolyte contained 10 mM sodium lactate as carbon source and was operated with self-circulation at a flow rate of 3 mL/min to shorten start-up process [34]. The detailed compositions of anolyte and catholyte have been described in our previous study [28]. During the start-up process, the anode and cathode were connected with an external resistor of 680 Ω. The MFC voltages were continuously monitored with a data acquisition system (USB-1608FS, Measurement Computing Corporation, USA) and the anolyte was regularly refreshed when the voltages decreased to 20 mV.

## 2.5 Biosensor tests

After being started up successfully, all the MFCs were fed with a continuous flow of anolyte during the biosensor test process. The flow rate remained the same while the concentration of sodium lactate was adjusted to 1 mM to improve sensor sensitivity [35]. The anolyte was amended with a specific concentration of chlortetracycline hydrochloride (CTC), avermectin (AVM) or mercury ion (as mercury sulfate, Hg[II]) to simulate different acute toxic shocks. A constant anode potential (0 mV *vs.* Ag/AgCl electrode) mode (CP mode) was used to enhance the sensor sensitivity [22, 29, 36]. Under this mode, the anode and the Ag/AgCl electrode were respectively connected to the working electrode and the reference electrode channels of a potentiostat (CHI1030C, ChenHua Inc., China), and the cathode served as a counter electrode. Each biosensor test included following steps and was conducted in duplicate. Firstly, all the MFCs were switched to operate under CP mode. Then, non-toxic anolyte was continuously pumped into the anodic chambers until the MFCs generated stable currents (fluctuation < 3%). After that, the influent was switched to toxic anolyte and the toxic exposure lasted for 30 min. Finally, the MFCs were switched to operate with a constant external resistor (680 Ω) and the influent was switched to non-toxic anolyte to obtain a fast recovery. The next test was conducted after the complete recovery of the MFCs. Finally, the inhibition ratios of MFC currents (CR) were calculated.

## 2.6 Biofilm viability analysis

After finishing the biosensor tests, all the MFCs got fully recovery and half MFCs (including one original MFC and one optimal MFC) were used to obtain the biofilm viability under a normal condition, while the other MFCs were used to investigate the biofilm viability after 30 min 1 mg/L CTC exposure. The viability of anodic biofilms was analyzed using a fluorescence staining method [28, 33]. The biofilms were stained with LIVE/DEAD® BacLight™ Bacterial Viability Kit (7012, Invitrogen, USA), which includes two dyes (SYTO®9 and PI) and can discriminate living and dead bacteria based on the integrity of cell membrane. The excitation/emission maxima for SYTO®9 and PI are 480/500 nm and 490/635 nm, respectively. After staining, the biofilm samples were observed *via* a confocal laser scanning microscope (CLSM, TCS SP8, Leica Microsystems Inc., Germany). During observation, each biofilm was divided into four regions (regions I-IV). Each region included four observation locations and its biofilm viability was determined by calculating the mean of the four locations.

## 2.7 Analysis

The hydrodynamic characteristics including $d_p$, $w_{min}$ and $v_c$ were obtained using CFD-post (Ansys Inc., USA) according to Eq. (6)-(8):

$$d_p = \frac{\{(x,y,z,)|u < u_{max} * 5\%\}}{\iiint dxdydz} \tag{6}$$

$$w_{min} = \frac{\iint wdxdy}{\iint dxdy} \tag{7}$$

$$v_c = \frac{\sqrt{\iint (w - w_{min})^2 dxdy}}{\iint wdxdy} \tag{8}$$

where u is the value of velocity in a flow field ($m \cdot s^{-1}$), $u_{max}$ is the maximum velocity in the flow field ($m \cdot s^{-1}$), w is the value of velocity at the anode surface ($m \cdot s^{-1}$). To evaluate the joint effects of the above hydraulic characteristics, a comprehensive hydraulic characteristic ($h_c$) was proposed and was defined as:

$$h_c = 0.4 d_{pnor} + 0.3 \times (-w_{minnor}) + 0.3 v_{cnor} \tag{9}$$

where $d_{pnor}$, $w_{minnor}$, $v_{cnor}$ are the standardized $d_p$, $w_{min}$ and $v_c$, respectively.

CR was employed to assess the sensor sensitivity for the detection of biotoxicity. CR was calculated using Eq. (10):

$$CR = {I_n - I_t}/{I_n} \times 100 \tag{10}$$

where $I_n$ and $I_t$ are the currents of an MFC before and after the toxic shock, respectively.

The viability of the biofilm (VB) was defined as the ratio of alive bacteria in total biomass and was calculated as:

$$VB = {}^{I_v}/_{(I_v + I_d)} * 100\% \quad (11)$$

where $I_v$ and $I_d$ are the integrated optical densities of alive and dead bacteria [8].

## 3. Results and Discussion

### 3.1 The anodic fluid field of the original MFC

The 3-D geometric model of the half fluid flow in the original MFC is shown in Fig. 1a. After mesh generation, a total of 289,649 nodes and 1,416,733 elements were obtained, and the average element size was 1.4E-5 mL (Fig. 1b). Further mesh refinement did not affect the simulation results, validating the mesh independence in our study. The flow pattern of the anodic fluid at an inlet flow rate of 3 mL/min (HRT ≅ 7 min) is visualized in Fig. 1c-d. The fluid flowed into the anodic chamber with a high velocity of more than 25 mm/min from the model bottom. As the fluid continued to flow into the cylindrical interior, a sharp decrease in the velocity was observed, and the fluid dispersed as a water-drop shape (Fig. 1c). When approaching the electrode, the pathway of the fluid changed drastically, and an obvious boundary layer was formed due to the fluid inertial force (Fig. 1c). The main flux rapidly diverged from the electrode and then converged towards the outlet. Although the carbon cloth was porous, its poor permeability led to a large flow resistance and extremely low flow velocities inside the electrode (Fig. 1d) [18].

Dead zone was defined as the region where the flow velocity was less than 5% of the maximum velocity ($u_{max}$) in the flow fluid [37]. According to the simulation results, an iso-surface where the flow velocity equaled to 5% of $u_{max}$ could be used to identify the dead zone in the anodic flow field. As shown in Fig. 1e, the dead zone was mainly located around the edge of the cylindrical interior. Notably, a clear bulge appeared at the iso-surface near the electrode (Fig. 1e), indicating the inhomogeneous distribution of the velocity at the anode surface. Specifically, the flow velocity was closer to 0 mm/min in the projective region of the inlet at the electrode surface, while it gradually increased to more than 0.3 mm/min along the surface (Fig. 1f). On the other hand, the $w_{min}$ at the electrode surface was only 0.26 mm/min, while the $v_c$ reached 43.1. The low velocity and its inhomogeneous distribution might result in the low availability of substrates, as well as the poor sensitivity to toxic shocks [14, 38]. Additionally, based on the results of CFD-post, the percentage of the dead zone in the flow field was up to 20.5%, which is detrimental to the recovery of an MFC-biosensor after a toxic shock due to the incomplete refreshment of anolyte [17]. Therefore, the configuration optimization is needed for the original MFC to improve its performance.

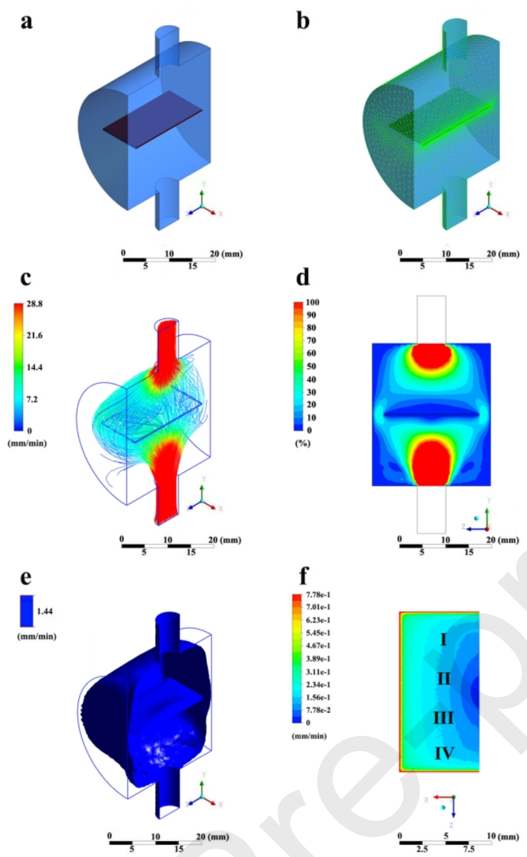


Fig. 1 3-D CFD simulation of the anode flow field of the original MFC: (a) geometric model of the anodic interior, (b) generated mesh, (c) flow pattern in the anodic chamber, (d) velocity distribution on the symmetry plane, (e) iso-surface with a velocity of 5% $u_{max}$, (f) velocity distribution at the electrode surface.

## 3.2 The effects of inlet/outlet settings and a serpentine flow field on the anodic flow field

Based on the hydrodynamic characteristics of the orthogonal design experiments (supplement material), it was notable that $d_p$ changed obviously among the different anodic configurations, indicating that the addition of baffle plates and the change of inlet/outlet positions are effective ways to decrease the proportion of dead zone. The impact of each optimizing factor on $d_p$ was further explored by range analysis and variance analysis (Table 1). From Table 1, the importance of all the factors on $d_p$ is $L_a \times L_e > L_a > L_b > G_r > L_e$, and the determination coefficient ($R^2$) of the model considering all the factors reached 0.999 based on the variance analysis. Among these factors, $L_a$, $L_b$ and $L_a \times L_e$ have significant effects on $d_p$ ($p<0.05$). Thus, an obvious interaction between $L_a$ and $L_e$ on $d_p$ is confirmed. Previous research has reported that the asymmetric locations of inlet/outlet were conducive to the reduction of dead zone [21]. Our study further demonstrates that the reasonable combination of baffle plates and inlet/outlet locations can further decrease the percentage of dead zone.

Table 1 Results of range analysis and variance analysis.

| | | $L_a$ | $L_e$ | $L_a \times L_e$ | $G_r$ | $L_b$ | Model |
|---|---|---|---|---|---|---|---|
| $d_p$ | K[a] | 4.6 | 0.5 | 7.3 | 1.4 | 2.7 | |
| | Sig.[b] | 0.001 | 0.623 | 0.041 | 0.180 | 0.019 | <0.001 |
| | | | | | | | $R^2$=0.999 |
| | Rank | | | $L_a \times L_e > L_a > L_b > G_r > L_e$ | | | |
| $w_{min}$ | K[a] | 0.09 | 0.74 | 0.98 | 0.23 | 0.50 | |
| | Sig.[b] | 0.920 | 0.049 | 0.949 | 0.686 | 0.277 | 0.056 |
| | | | | | | | $R^2$=0.920 |
| | Rank | | | $L_a \times L_e > L_e > L_b > G_r > L_a$ | | | |
| $v_c$ | K[a] | 3.7 | 14.5 | 18.7 | 3.1 | 1.3 | |
| | Sig.[b] | 0.184 | 0.001 | 0.546 | 0.390 | 0.840 | <0.001 |
| | | | | | | | $R^2$=0.998 |
| | Rank | | | $L_a \times L_e > L_e > L_a > G_r > L_b$ | | | |
| $h_c$ | K[a] | 0.16 | 0.07 | 0.30 | 0.08 | 0.05 | |
| | Sig.[b] | 0.002 | 0.041 | 0.015 | 0.089 | 0.337 | <0.001 |
| | | | | | | | $R^2$=0.992 |
| | Rank | | | $L_a \times L_e > L_a > G_r > L_e > L_b$ | | | |

[a]K is the range of a specific indicator under different levels of factors obtained by range analysis.

[b]Sig. is the p-value for a certain factor obtained by variance analysis. Sig. < 0.05 is denoted as the significant level.

Anodic configurations also have an important influence on the flow velocity at the anode surface. $L_a \times L_e$ is the main factor affecting the $w_{min}$ at the electrode surface, followed by $L_e$, and $L_a$ is the last (Table 1). More than 92% of the total variance of $w_{min}$ can be interpreted by the model containing all the factors, and $L_e$ has a significant impact on $w_{min}$. By adding two 20 mm × 20 mm × 2 mm baffle plates, $w_{min}$ sharply increased from 0.26 mm/min to 1.00 mm/min while the $v_c$ dramatically decreased from 42.5 to 28.0, suggesting that a serpentine flow field can improve the flow velocity at the anode surface as well as enhance the homogeneity of the velocity distribution. Previous studies have found that setting baffles can improve the efficiency of wastewater treatment bioreactors [39-42]. Our study further provides a visualization of the effect of baffles on a flow field and quantifies their influence on flow velocity, which probably contributes to the interpretation of the enhanced performance reported in the previous research.

According to the orthogonal test results, the minimum $d_p$ was obtained at the fifteenth experiment while both the maximum $w_{min}$ and minimum $v_c$ were observed at the eighth experiment. Therefore, a weighted method was introduced to calculate the comprehensive hydraulic characteristic $h_c$ and to obtain the optimal configuration. Detailed weighted calculation process is shown in Eq. (9), and a lower $h_c$ indicates that the anode hydrodynamics might be more favorable for the enhancement of MFC performance. As shown in Table 1, the order of the effects of the optimized factors on $h_c$ is $L_a \times L_e > L_a > G_r > L_e > L_b$, and the model can explain 99.2% of the variation in $h_c$. In addition, $L_a$, $L_e$ and their interaction have a significant influence on $h_c$. Accordingly, the optimal level of each factor was determined as $L_a$ of 9.25 mm, $L_e$ of 20 mm, $L_b$ of 7.5 mm and $G_r$ of -5 °, respectively.

3.3 The anodic fluid field of the optimal MFC

The anodic fluid field of the optimal MFC was visualized with the same CFD simulation parameters (Fig. 2). Different from the flow pattern in the original MFC, the main flux occurred along the baffles in the optimal MFC and an obvious flow acceleration was observed at the end of the baffles, which was in accordance with the previous studies [15, 43-46]. Due to the distinct flow pathway, the hydrodynamic characteristics of the optimal MFC were obviously different from those of the original MFC. Through the configuration optimization, $d_p$ decreased by 14.1% (from 20.5% to 17.6%) and $w_{min}$ increased by 334.6% (from 0.26 mm/min to 1.13 mm/min), while $v_c$ decreased by 24.8% (from 43.1 to 32.4). Moreover, the comprehensive hydraulic characteristic $h_c$ reduced to -0.04, indicating that the optimized configuration might be more favorable for the electricity generation and the biotoxicity detection of an MFC.

A few studies have reported that miniaturizing the anodic chamber or increasing the influent flow rate can improve the velocity at anode surface [22, 47]. However, an excessive small anodic chamber not only increases the difficulty of MFC fabrication, but also affects the effective area of PEM and the ratio between cathode to anode [48], which might cause deterioration to MFC performance. In this study, an alternative solution was proposed to solve this problem. Using a serpentine flow field and appropriate inlet/outlet settings, the flow velocity at the anode surface greatly increased, as well as the percentage of dead zone reduced. According to the kinetics of electrode process, a higher surface velocity can facilitate the migration of target substances (organic matter or toxicants) from anolyte into a biofilm [17, 18]. Thus, the MFCs with the optimal configuration are expected to deliver better electricity performance and higher sensor sensitivity towards water quality monitoring.

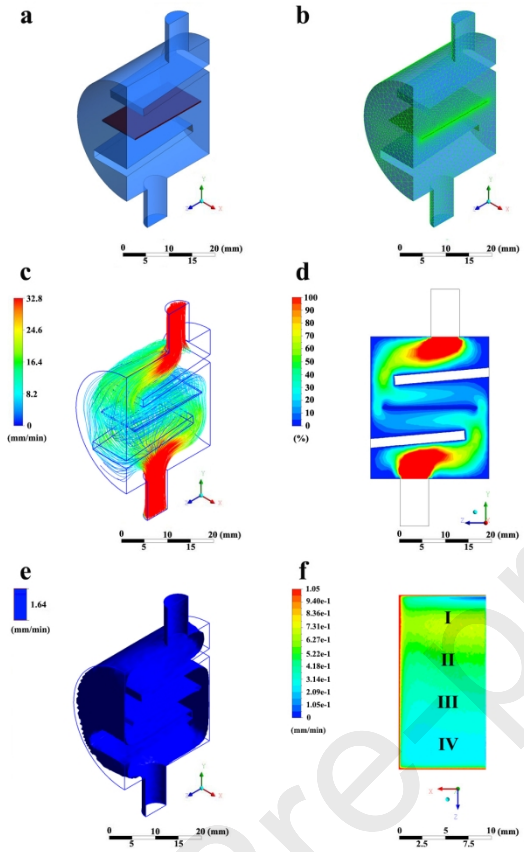


Fig. 2 3-D CFD simulation of the anode flow field of the optimal MFC: (a) geometric model of the anodic interior, (b) generated mesh, (c) flow pattern in the anodic chamber, (d) velocity distribution on the symmetry plane, (e) iso-surface with a velocity of 5% $u_{max}$, (f) velocity distribution at the electrode surface.

### 3.4 The effect of the optimal configuration on MFC-Biosensor performance

To verify the above conjecture, two optimal MFCs and two original MFCs were constructed. Compared with the original MFC, $L_a$ of the optimal MFC was changed from 12.50 mm to 9.25 mm, and two baffles both with a size of 20 mm × 20 mm × 2 mm were inserted into the anodic chamber. Each baffle was 7.5 mm away from the carbon cloth and inclined to the electrode by 5° (Fig. 3). The cathode chambers and PEMs were identical in both types of MFCs.

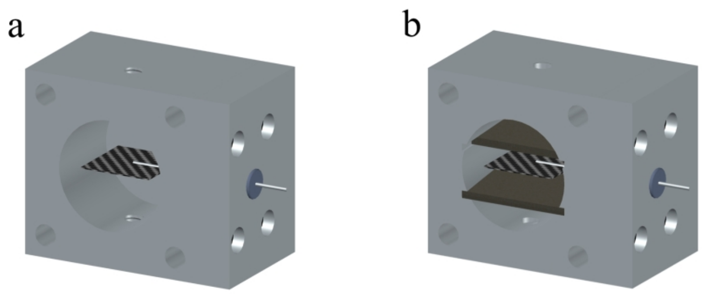


Fig. 3 The 3D model of the anodic chambers with the original configuration (a) and the optimal

configuration (b).

The output voltages of the two type MFCs during the start-up process are shown in Fig. 4a. Notably, the MFCs generated obvious voltages after inoculation and the first voltage peak occurred in a very short time, testifying that *S. loihica* PV-4 can generate obvious current without the formation of biofilm [28]. With the enrichment of the anodic biofilms, the maximum voltages of all the MFCs in each batch gradually increased and finally stabilized after the fourth batch (the deviation of maximum voltages between two batches within 5%). However, obvious differences in the output voltages between the two type MFCs can be observed. The stable voltages of the optimal MFCs achieved 205.0±5.5 mV while those of the original MFCs were only 166.5±8.3 mV, indicating that the electricity generation is enhanced after the configuration optimization.

After the start-up process, all the MFCs were challenged with three types of toxic shocks, including 1 mg/L CTC, 1 mg/L AVM and 1 mg/L Hg[II]. The responses of the two type MFCs to various toxic shocks are shown in supplementary material. By comparing the CR values under the same toxic shock, it was noted that the optimal MFCs present higher sensitivity to detect biotoxicity than the original MFCs. Specifically, the CR values of the optimal MFCs reached 36.2±3.0% (CTC), 24.4±2.7% (AVM) and 32.9±5.5% (Hg[II]) while those of the original MFCs were only 25.5±1.2% (CTC), 16.7±3.2% (AVM) and 21.6±3.8% (Hg[II]) (Fig. 4b). Considering that the employment of CR to evaluate sensor sensitivity can eliminate the interference of baseline signal [8, 49], it was concluded that the configuration optimization can not only enhance the MFC electricity generation, but also enhance the sensitivity of MFCs to toxicants.

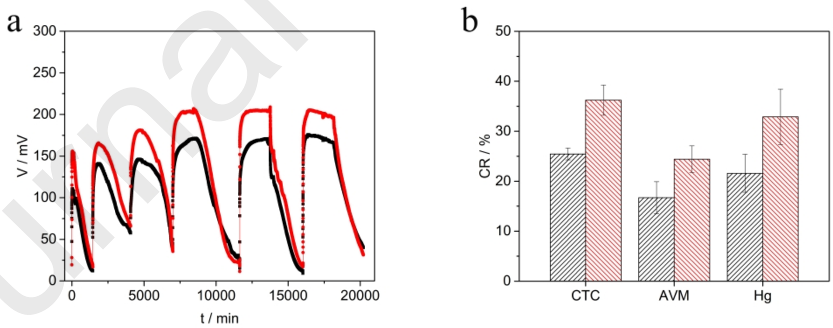


Fig. 4 Effect of optimal configuration on MFC performance: (a) evolution of MFC voltage during start up process; (b) CR values of different pollutants. (Black and red colors represent original and optimal MFCs, respectively.)

3.5 The biological mechanism of the enhanced performance with the optimal configuration

To explore the biological mechanism of the effects of optimal configuration on sensor performance, CLSM analysis was used to reveal the biofilm viability under a normal condition and its changes induced by a CTC shock. Biomass is an important factor influencing MFC current generation and it can be estimated by the integrated optical density (IOD) of green color (represents living cells) in CLSM image. Notably, an obvious difference of IOD was observed between two type MFCs, and the IOD of the optimal MFC biofilm was 33.3% higher than that of the original MFC biofilm, indicating an increase in biomass density through the configuration optimization. Considering that the higher flow velocity and its better homogeneity at the electrode surface of the optimal MFC, it was concluded that higher biomass density and enhanced mass transport might lead to the superior electrochemical activity and a higher generated current in the optimal MFC (Fig. 4a) [19, 32].

On the other hand, the electrode surfaces were almost completely covered by alive bacteria under the normal condition [8, 29], and the average biofilm viability was similar for the original (95.3±0.7%) and optimal MFCs (95.1±1.9%) (Fig. 5a). However, a large number of dead bacteria appeared at the electrode surfaces after the 30 min exposure to CTC, verifying the acute toxicity of CTC. Notably, the biofilm viability decreased by 25.6±7.1% after the CTC shock in the optimal MFCs, while it only dropped by 16.9±4.8% in the original MFCs (Fig. 5a). This phenomenon indicates that the effect of toxicant on biofilm viability is much larger in the optimal MFC. Thus, the optimal MFC delivers higher CRs and better sensitivity to toxic shocks (Fig. 4b).

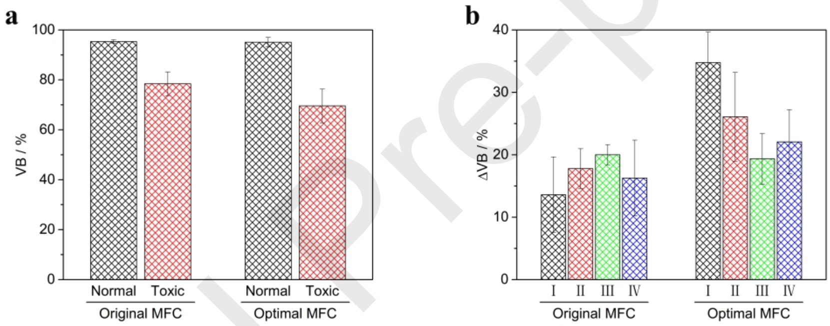


Fig. 5 The effects of a CTC shock on biofilm viability: (a) total biofilm viability of the original and optimal MFC-Biosensors before and after a CTC shock; (b) the change of biofilm viability in each electrode region.

Furthermore, the spatial changes of biofilm viability decrease followed different patterns between the two type MFCs. For the electrode surface of the original MFC, the decreases of biofilm viability in the regions II and III were 17.8±3.2% and 20.0±1.6%, which were slightly higher than those in regions I (13.6±6.1%) and IV (16.3±6.1%) (Fig. 5b). This phenomenon is probably due to the fact that the higher flow velocity in the regions II-III (Fig. 1f). As for the optimal MFC, the largest decrease of biofilm viability was observed in region I (34.8±4.9%), where the highest flow velocity appeared (Fig. 2f). While in the rest regions of the electrode surface, as the surface velocity gradually declined from regions II to IV, the biofilm viability accordingly decreased to 26.1±7.1%, 19.4±4.1% and 22.1±5.2%, respectively (Fig. 5b). These results demonstrated that a higher flow velocity at the electrode surface is conducive to the permeation of toxicants into anodic biofilms and improves sensor sensitivity.

## 4. Conclusions

In this study, the anodic flow field and hydrodynamic characteristics of a common dual-chamber MFC were analyzed *via* CFD simulations, and the optimal configuration was obtained with orthogonal design. Compared with the original configuration, the percentage of dead zone reduced by 14.1%, while the flow velocity at electrode surface and its uniformity improved by 334.6% and 24.8% through optimization, respectively. Moreover, with the optimal configuration, the electricity generation and the sensor sensitivity enhanced by 23.1% and 46.1-52.3%, respectively. By the joint analysis of hydrodynamics and biofilm viability, the enhanced sensitivity was attributed to the fact that the improved flow velocity facilitates the permeation of toxicants into biofilms.

Acknowledgements

This work was financially supported by grants from the National Natural Science Foundation of China [31770135]; and the Fundamental Research Funds for the Central Universities. Thank Dr Wenjia Wang for her guidance and suggestions on the CFD simulation in this study.

Notes

The authors declare no competing financial interest.

References

1. Logan, B.E., Hamelers, B., Rozendal, R.A., Schröder, U., Keller, J., Freguia, S., Aelterman, P., Verstraete, W., Rabaey, K., 2006. Microbial fuel cells: Methodology and technology. Environ. Sci. Technol. 40, 5181-5192.
2. Nimje, V.R., Chen, C.Y., Chen, H.R., Chen, C.C., Huang, Y.M., Tseng, M.J., Cheng, K.C., Chang, Y.F., 2012. Comparative bioelectricity production from various wastewaters in microbial fuel cells using mixed cultures and a pure strain of *Shewanella oneidensis*. Bioresour. Technol. 104, 315-323.
3. Xie, B.Z., Liu, B.J., Yi, Y., Yang, L.G., Liang, D.W., Zhu, Y., Liu, H., 2016. Microbiological mechanism of the improved nitrogen and phosphorus removal by embedding microbial fuel cell in anaerobic–anoxic–oxic wastewater treatment process. Bioresour. Technol. 207, 109-117.
4. Kim, B.H., Chang, I.S., Gil, G.C., Park, H.S., Kim, H.J., 2003a. Novel BOD (biological oxygen demand) sensor using mediator-less microbial fuel cell. Biotechnol. Lett. 25, 541-545.
5. Kim, M., Youn, S.M., Shin, S.H., Jang, J.G., Han, S.H., Hyun, M.S., Gadd, G.M., Kim, H.J., 2003b. Practical field application of a novel BOD monitoring system. J. Environ. Monit. 5, 640-643.
6. Wang, D.L., Liang, P., Jiang, Y., Liu, P.P., Miao, B., Hao, W., Huang, X., 2018. Open external circuit for microbial fuel cell sensor to monitor the nitrate in aquatic environment. Biosens. Bioelectron. 111, 97-101.
7. Yang, Y., Yu, Y.Y., Shi, Y.T., Moradian, J.M., Yong, Y.C., 2019. In vivo two-way redox cycling system for independent duplexed electrochemical signal amplification. Anal. Chem. 91, 4939-4942.
8. Li, T., Wang, X., Zhou, L., An, J.K., Li, J.H., Li, N., Sun, H.W., Zhou, Q.X., 2016. Bioelectrochemical sensor using living biofilm to in situ evaluate flocculant toxicity. ACS Sens. 1, 1374-1379.
9. Kim, M., Hyun, M.S., Gadd, G.M., Kim, H.J., 2007. A novel biomonitoring system using microbial fuel cells. J. Environ. Monit. 9, 1323-1328.

10. Yang, Y., Fang, Z., Yu, Y.Y., Wang Y.Z., Naraginti, S., Yong, Y.C., 2019. A mediator-free whole-cell electrochemical biosensing system for sensitive assessment of heavy metal toxicity in water. Water Sci. Technol. 79, 1071-1080.
11. Yang, Y., Wang, Y.Z., Fang, Z., Yu, Y.Y., Yong, Y.C., 2018. Bioelectrochemical biosensor for water toxicity detection: generation of dual signals for electrochemical assay confirmation. Anal. Bioanal. Chem. 410, 1231-1236.
12. Kumar, R., Singh, L., Zularisam, A.W., Hai, F.I., 2018. Microbial fuel cell is emerging as a versatile technology: a review on its possible applications, challenges and strategies to improve the performances. Int. J. Energ. Res. 42, 369-394.
13. Zhou, T.Y., Han, H.W., Liu, P., Xiong, J., Tian, F.K., Li, X.K., 2017. Microbial fuels cell-based biosensor for toxicity detection: A review. Sensors 17, 2230.
14. Jiang, Y., Yang, X.F., Liang, P., Liu, P.P., Huang, X., 2018. Microbial fuel cell sensors for water quality early warning systems: Fundamentals, signal resolution, optimization and future challenges. Renew. Sustain. Energy Rev. 81, 292-305.
15. Kim, J., Kim, H., Kim, B., Yu, J., 2014. Computational fluid dynamics analysis in microbial fuel cells with different anode configurations. Water Sci. Technol. 69, 1447-1452.
16. Vilà-Rovira, A., Puig, S., Balaguer, M.D., Colprim, J., 2015. Anode hydrodynamics in bioelectrochemical systems. RSC Adv. 5, 78994-79000.
17. Moon, H., Chang, I.S., Jang, J.K., Kim, B.H., 2005. Residence time distribution in microbial fuel cell and its influence on COD removal with electricity generation. Biochem. Eng. J. 27, 59-65.
18. Wang, Y.Z., Wang, Y.K., He, C.S., Yang, H.Y., Sheng, G.P., Shen, J.Y., Mu, Y., Yu, H.Q., 2015. Hydrodynamics of an electrochemical membrane bioreactor. Sci. Rep. 5, 10387.
19. Kim, J.R., Boghani, H.C., Amini, N., Aguey-Zinsou, K.F., Michie, I., Dinsdale, R.M., Guwy, A.J., Guo, Z.X., Premier, G.C., 2012. Porous anodes with helical flow pathways in bioelectrochemical systems: The effects of fluid dynamics and operating regimes. J. Power Sources 213, 382-390.
20. Krieg, T., Wood, J.A., Mangold, K.M., Holtmann, D., 2018. Mass transport limitations in microbial fuel cells: Impact of flow configurations. Biochem. Eng. J. 138, 172-178.
21. Massaglia, G., Gerosa, M., Agostino, V., Cingolani, A., Sacco, A., Saracco, G., Margaria, V., Quaglio, M., 2017. Fluid dynamic modeling for microbial fuel cell based biosensor optimization. Fuel Cells 17, 627-634.
22. Jiang, Y., Liang, P., Zhang, C.Y., Bian, Y.H., Yang, X.F., Huang, X., Girguis, P.R., 2015. Enhancing the response of microbial fuel cell based toxicity sensors to Cu(II) with the applying of flow-through electrodes and controlled anode potentials. Bioresour. Technol. 190, 367-372.
23. Quaglio, M., Massaglia, G., Vasile, N., Margaria, V., Chiodoni, A., Salvador, G.P., Marasso, S.L., Cocuzza, M., Saracco, G., Pirri, F.C., 2019. A fluid dynamics perspective on material selection in microbial fuel cell-based biosensors. Int. J. Hydrog. Energy 44, 4533-4542.

24. Logan, B.E., Wallack, M.J., Kim, K.Y., He, W.H., Feng, Y.J., Saikaly, P.E., 2015. Assessment of microbial fuel cell configurations and power densities. Environ. Sci. Technol. Lett. 2, 206-214.
25. Zhou, J., Zhang, L., Li, J., Ye, D.D., Zhu, X., 2014. Experimental research of mass transfer in anode of microbial fuel cells with serpentine flow fields. Chinese J. Power Sources 38, 57-59.
26. White, F. M., 2015. Fluid Mechanics, 8th ed. McGraw-Hill Education, Los Angeles.
27. Nield, D.A., 1983. The boundary correction for the Rayleigh-Darcy problem: Limitations of the brinkman equation. J. Fluid Mech. 128, 37-46.
28. Yi, Y., Xie, B.Z, Zhao, T., Liu, H., 2018. Comparative analysis of microbial fuel cell based biosensors developed with a mixed culture and *Shewanella loihica* PV-4 and underlying biological mechanism. Bioresour. Technol. 265, 415-421.
29. Yi, Y., Xie, B.Z., Zhao, T., Qian, Z.N., Liu, H., 2019. Effect of control mode on the sensitivity of a microbial fuel cell biosensor with *Shewanella loihica* PV-4 and the underlying bioelectrochemical mechanism. Bioelectrochemistry 128, 109-117.
30. Wang, S.X., Wang, Y.L., 2016. Investigation of the through-plane effective oxygen diffusivity in the porous media of PEM fuel cells: Effects of the pore size distribution and water saturation distribution. Int. J. Heat Mass Transf. 98, 541-549.
31. Tomadakis, M.M., Robertson, T.J., 2005. Viscous permeability of random fiber structures: comparison of electrical and diffusional estimates with experimental and analytical results. J. Compos. Mater. 39, 163-188.
32. Zhao, L., Li, J., Battaglia, F., He, Z., 2016. Investigation of multiphysics in tubular microbial fuel cells by coupled computational fluid dynamics with multi-order Butler–Volmer reactions. Chem. Eng. J. 296, 377-385.
33. Sun, D., Cheng, S.A., Wang, A.J., Li, F.J., Logan, B.E., Cen, K.F., 2015. Temporal-spatial changes in viabilities and electrochemical properties of anode biofilms. Environ. Sci. Technol. 49, 5227-5235.
34. Ye, Y.Y., Ngo, H.H., Guo, W.S., Liu, Y.W., Chang, S.W., Nguyen, D.D., Ren, J.W., Liu, Y., Zhang, X.B., 2019. Feasibility study on a double chamber microbial fuel cell for nutrient recovery from municipal wastewater. Chem. Eng. J. 358, 236-242.
35. Jiang, Y., Liang, P., Liu, P.P., Bian, Y.H., Miao, B., Sun, X.L., Zhang, H.L., Huang, X., 2016. Enhancing signal output and avoiding BOD/toxicity combined shock interference by operating a microbial fuel cell sensor with an optimized background concentration of organic matter. Int. J. Mol. Sci. 17, 1392.
36. Stein, N.E., Hamelers, H.V.M., Buisman, C.N.J., 2012. The effect of different control mechanisms on the sensitivity and recovery time of a microbial fuel cell based biosensor. Sens. Actuators B: Chem. 171, 816-821.
37. Vesvikar, M.S., Al-Dahhan, M., 2005. Flow pattern visualization in a mimic anaerobic digester using CFD. Biotechnol. Bioeng. 89, 719-732.
38. Newton, G.J., Mori, S., Nakamura, R., Hashimoto, K., Watanabe, K., 2009. Analyses of current-generating mechanisms of *Shewanella loihica* PV-4 and

*Shewanella oneidensis* MR-1 in microbial fuel cells. Appl. Environ. Microbiol. 75, 7674-7681.

39. Liu, J.D., Tian, C., Jia, X.L., Xiong, J.X., Dong, S.N., Wang, L., Bo, L.L., 2017. The brewery wastewater treatment and membrane fouling mitigation strategies in anaerobic baffled anaerobic/aerobic membrane bioreactor. Biochem. Eng. J. 127, 53-59.
40. Al-Mamun, A., Baawain, M.S., Egger, F., Al-Muhtaseb, A.H., Ng, H.Y., 2017. Optimization of a baffled-reactor microbial fuel cell using autotrophic denitrifying bio-cathode for removing nitrogen and recovering electrical energy. Biochem. Eng. J. 120, 93-102.
41. Li, Z.L., Yao, L., Kong, L.C., Liu, H., 2008. Electricity generation using a baffled microbial fuel cell convenient for stacking. Bioresour. Technol. 99, 1650-1655.
42. Liu, H.P., Zhang, B.G., Liu, Y., Wang, Z.J., Hao, L.T., 2015. Continuous bioelectricity generation with simultaneous sulfide and organics removals in an anaerobic baffled stacking microbial fuel cell. Int. J. Hydrog. Energy 40, 8128-8136.
43. de Lamotte, A., Delafosse, A., Calvo, S., Toye, D., 2018. Identifying dominant spatial and time characteristics of flow dynamics within free-surface baffled stirred-tanks from CFD simulations. Chem. Eng. Sci. 192, 128-142.
44. Li, C., Xia, J.Y., Chu, J., Wang, Y.H., Zhuang, Y.P., Zhang, S.L., 2013. CFD analysis of the turbulent flow in baffled shake flasks. Biochem. Eng. J. 70, 140-150.
45. Monfared, M.A., Kasiri, N., Salahi, A., Mohammadi, T., 2012. CFD simulation of baffles arrangement for gelatin-water ultrafiltration in rectangular channel. Desalination 284, 288-296.
46. Wang, S., Luo, K., Hu, C.S., Fan, J.R., 2019. CFD-DEM study of the effect of ring baffles on system performance of a full-loop circulating fluidized bed. Chem. Eng. Sci. 196, 130-144.
47. Di Lorenzo, M., Thomson, A.R., Schneider, K., Cameron, P.J., Ieropoulos, I., 2014. A small-scale air-cathode microbial fuel cell for on-line monitoring of water quality. Biosens. Bioelectron. 62, 182-188.
48. Uría, N., Sánchez, D., Mas, R., Sánchez, O., Munoz, F.X., Mas, J., 2012. Effect of the cathode/anode ratio and the choice of cathode catalyst on the performance of microbial fuel cell transducers for the determination of microbial activity. Sens. Actuators B: Chem. 170, 88-94.
49. Wang, X., Gao, N.S.J., Zhou, Q.X., 2013. Concentration responses of toxicity sensor with *Shewanella oneidensis* MR-1 growing in bioelectrochemical systems. Biosens. Bioelectron. 43, 264-267.